Heterogeneous ATP patterns in microvascular networks

Zhe Gou, Hengdi Zhang, Chaouqi Misbah

Heterogeneous ATP patterns in microvascular networks

Zhe Gou,[1] Hengdi Zhang,[1,2] and Chaouqi Misbah[1,*]

[1] *Université Grenoble Alpes, CNRS, LIPhy, F-38000 Grenoble, France*

[2] *Shenzhen Sibionics Co. Ltd., Shenzhen, China*

Abstract

ATP is not only an energy carrier but also serves as an important signaling molecule in many physiological processes. Abnormal ATP level in blood vessel is known to be related to several pathologies, such as inflammation, hypoxia, and atherosclerosis. Using advanced numerical methods we analyzed ATP released by red blood cells (RBCs) and its degradation by endothelial cells (EC) in a cat mesentery-inspired vascular network, accounting for RBCs mutual interaction and interactions with vascular walls. Our analysis revealed a heterogeneous ATP distribution in the network, with higher concentrations in the cell-free layer, concentration peaks around bifurcations, and heterogeneity among vessels of the same level. These patterns arise from the spatiotemporal organization of RBCs induced by the network geometry. It is further shown that an alteration of hematocrit and flow strength significantly affect ATP level as well as heterogeneity in the network, with potential impact on Ca^{2+} signaling in ECs. These findings constitute a first building block to elucidate the intricate nature of ATP patterns in vascular networks and its far reaching consequences for other biochemical signaling, such as calcium, by ECs.

* chaouqi.misbah@univ-grenoble-alpes.fr

I. INTRODUCTION

Extracellular ATP plays an important role in the regulation of vascular resistance [1–6]. In arterioles, high ATP concentration can trigger intracellular Ca^{2+} signaling of endothelial cells (ECs) [7, 8], eventually leading to vasodilation [9–11]. At the capillary level, vascular diameter can be altered thanks to ATP-induced pericyte relaxation [12, 13]. In blood vessels, the main contribution of ATP level originates from red blood cells (RBCs). In vitro experiments have shown that ATP release by RBCs can be stimulated by shear stress and by RBCs shape deformation [14–18]. Two different pathways of ATP release by RBCs have been put forward: (a) the pannexin 1 (Px1) hemichannel [19] which is sensitive to mechanical stress [20, 21], and (b) the cystic fibrosis transmembrane conductance regulator (CFTR) [22] which is affected by the deformation of cell membrane [15, 18, 23]. More precisely, Px1 channel is considered as the main candidate for transmembrane ATP release, and CFTR acts as a regulator of the Px1 channel [18]. Based on these two ATP release mechanisms, a theoretical model has been developed and validated recently [24]. Numerical simulations showed quantitative agreements with in vitro experiments [18] for ATP release for a dilute suspension of RBCs in a straight channel.

Apart from RBCs, ECs also contribute to ATP level in vascular networks. By forming a monolayer on the inner surface of blood vessels, ECs are involved in a wide range of response to hemodynamic shear stress, including activation of ion channels [25, 26], remodeling of cellular morphology [27–29], and intracellular Ca^{2+} oscillations [30, 31], etc. ECs affect ATP concentration from two different aspects. On the one hand, experiments have shown that shear stress elicits ATP release by ECs [3, 32–34], which is believed to be the starting point of flow-induced regulation in microcirculation. On the other hand, once ATP is released into the extracellular milieu, it can be degraded rapidly to ADP, AMP, and adenosine by ecto-enzymes [35, 36]. These membrane-associated ecto-enzymes at the EC surface act as regulators so that the extracellular ATP concentration on vascular ECs remains at a level of nanomolar (nM) [37, 38], preventing thus pathological processes, such as inflammation, cell proliferation, and atherosclerosis [39].

In vivo vascular networks are quite complex, and are composed of a cascade of bifurcations, including both diverging and converging geometries. Near these bifurcations, the change of flow dynamics is known to cause a variety of phenomena, such as cell partitioning

[40–44] and cell/particle adhesion [45–47]. The morphology of ECs is also affected, due to the change of shear stress at those sites [48]. Moreover, the nucleotide concentration in the endothelium shows heterogeneous distribution around bifurcations [49, 50]. In a complex geometry like microvascular network, several features regarding blood flow and biochemical signaling are reported. For example, it has been observed experimentally and numerically that the partitioning of RBCs in downstream bifurcations is affected by the flow in upstream bifurcations [51, 52]. Due to the complex structure of microvascular networks, a heterogeneous distribution of cells is observed [53], affecting chemical signaling as well as oxygen transport [54]. These observations constitute a motivation for analyzing ATP signaling in a vascular network.

In our recent work, ATP release by a single RBC under shear flow, Poiseuille flow, and bifurcation flow were studied numerically [24]. Using the same ATP release model, a follow-up study revealed a maximal ATP release for specific hematocrit under Poiseuille flow [55]. An indefinite increase of ATP concentration was observed, since the ATP degradation by ECs was not taken into account. Furthermore, the vessels in these two studies are quite simple, either straight channels or Y-shape bifurcating channels. Although we have shown that a diverging bifurcation is beneficial to ATP release [24], systematic studies in a complex vessel network are still lacking.

In this paper, we show the emergence of a steady state ATP pattern in a microvascular network when ECs are taken into account. We further reveal that this ATP pattern is related to heterogeneous distribution of RBCs as they flow through the network. The effects of flow strength and hematocrit on ATP patterns are also studied systematically. A remarkable feature reported here is that ATP present peaks at network bifurcations. The rest of the paper is organized as follows. In Section II, we give a brief description of the simulation set up, followed with the ATP release/degradation models for RBCs and ECs. Then we present the main findings in Section III, which focuses on the steady state ATP pattern in a vascular network. The mechanism and influencing factors behind the complex ATP patterns are discussed. Conclusion and perspectives are presented in Section IV.

II. METHOD

The numerical model has been introduced and validated in our previous works [24, 55–

57]. The details of the model are presented therein. In the present study, we further consider ATP release and degradation by ECs. Hereafter we give a brief overview of simulation set up and ATP kinetics modeling.

A. Simulation set up

This study is carried out under 2D configuration. This simplification has been validated by our recent study which shows a qualitative agreement with 3D simulations [55]. The flow geometry is mapped from a microvascular network extracted from Ref. [58], as shown in Figure 1, which is a cat mesentery-inspired network. The network contains 22 vessels labeled as "V1–22", of which the diameters range from 7–23 μm, and 14 bifurcations labeled as "B1–14". The vessels after diverging bifurcations are categorized into three different levels: level I for V2–3, level II for V4–7, and level III for V8–15. The flow is imposed by a pressure gradient along the flow direction (from left to right). Periodic boundary conditions are used at the inlet and the outlet, which are extended long enough to avoid numerical artifacts due to periodicity. Other boundaries (solid lines in Figure 1) correspond to vascular network walls which are assumed to be lined with a monolayer of ECs.

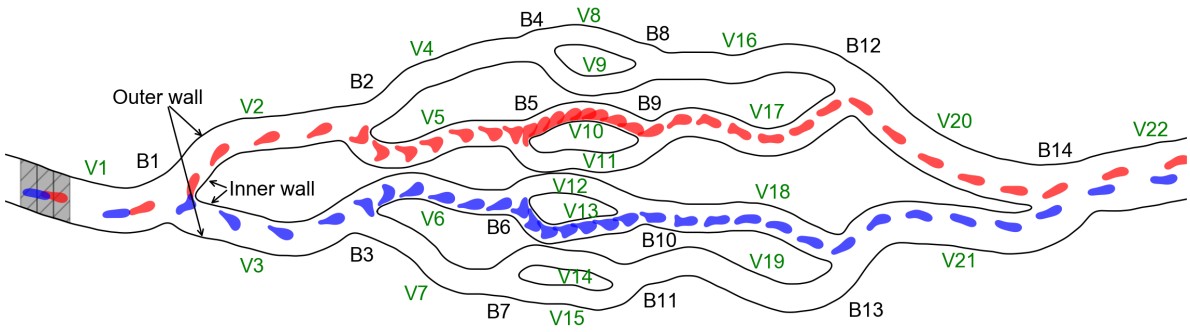

FIG. 1. A snapshot of the microvascular network. Bifurcations are labeled as "B1–14", while vessels as "V1–22". The inner and outer walls are defined around bifurcations. For data analysis purpose, the network is divided into several boxes, as the shaded area shows. We show the time series of two selected RBCs (blue and red) in a suspension of $Ht = 10\%$ with $Ca = 16.7$.

Blood is modeled as a suspension of RBCs immersed in plasma of viscosity $\mu = 0.001$ Pa·s. Each RBC is treated as a cytosol drop with a characteristic radius $R_0 = 3$ μm (the radius of the circle having the same area as that of RBC), enclosed by an elastic membrane.

Its shape deflation is described by reduced area $\tau = 4\pi A/P^2$, where A is its area and P is its perimeter. We fix $\tau = 0.65$ in this study, in reference to the known value of a healthy RBC. Cytosol viscosity is approximately 6 times greater than plasma viscosity, set as 0.006 Pa·s. RBC membrane elasticity is described by the Helfrich energy [59], taking into account bending mode with a bending modulus $k_b = 3 \times 10^{-19}$ J and the constraint of local membrane inextensibility. The force due to membrane deformation is then calculated thanks to functional derivative of membrane bending energy [60, 61].

ATP is modeled as a solute in plasma. The concentration of ATP, denoted by a, diffuses with diffusion coefficient $D_{ATP} = 2.36 \times 10^{-10}$ m^2/s [62], and is advected by the flow. The ATP release or degradation by RBCs and ECs are considered as flux on cell membranes, and the mathematical models will be given later.

In the present study, the effects of hematocrit and flow strength on ATP kinetics are investigated. Hematocrit Ht is defined as the area fraction of RBCs in the network. Flow strength is characterized by capillary number $Ca = \mu\dot{\gamma}_w R_0^3/k_b$, where $\dot{\gamma}_w$ is the undisturbed shear rate on the boundaries of vessel V1 (i.e. without RBCs). The mean velocities and the wall shear stresses in vessel V1 at different capillary numbers are listed in Table I.

Table I. Conversion between capillary number and physiological numbers

Ca	Mean velocity (mm/s)	Wall shear stress* (Pa)
11.5	0.35	0.128
16.7	0.5	0.185
33.4	1.0	0.371
50.1	1.5	0.556

*Estimated using plasma viscosity.

B. ATP release by RBCs

ATP release by RBCs is characterized by the phenomenological model proposed by Zhang *et al.* [24]. The intracellular ATP is released through Px1 channel, which is a mechanosen-

sitive channel, due to membrane shear stress as

$$p_\sigma = k_\sigma \cdot H(\sigma_{mem} - \sigma_c). \tag{1}$$

Here p_σ is the ATP flux through Px1 channel, k_σ is the ATP release coefficient, H is the Heaviside function, σ_{mem} is the membrane shear stress, and σ_c is the critical shear stress beyond which Px1 channel is activated. The membrane shear stress is defined as $\sigma_{mem} = \mu_{ex}|\partial u_{\boldsymbol{t}}/\partial \boldsymbol{n}|$, where $u_{\boldsymbol{t}}$ is the velocity tangential to the membrane, and $\boldsymbol{n}$ is the outward normal vector. CFTR is activated by deformation-induced free actin. It further regulates the Px1 channel by an amplifying factor as

$$p_{\dot{c}} = min(1 + k_{\dot{c}} \cdot (\dot{c} - \dot{c}_c) \cdot H(\dot{c} - \dot{c}_c), p_{\dot{c}_{max}}), \tag{2}$$

where $k_{\dot{c}}$ is the phenomenological coefficient, $\dot{c}$ and $\dot{c}_c$ are the instantaneous and critical curvature change rate respectively, and $p_{\dot{c}_{max}}$ is the upper limit for CFTR activation. The instantaneous curvature change rate is defined as the Lagrangian derivative of local curvature $\dot{c} = |dc/dt|$. The combination of the two effects (i.e. shear-inuded Px1 activation and membrane deformation) defines the local ATP release rate on membrane as

$$\psi_{RBC} = p_\sigma p_{\dot{c}}. \tag{3}$$

The ATP flux across cell membrane is written as

$$D_{ATP}\frac{\partial a}{\partial \boldsymbol{n}} = -\psi_{RBC}. \tag{4}$$

The model parameters are fitted by experimental results in [18], as shown in Table II. For a given RBC, we define the ATP release level as

$$\psi^* = \frac{1}{k_\sigma P}\int_0^P \psi_{RBC} ds, \tag{5}$$

which describes the dimensionless ATP release rate of that cell.

C. ATP flux at ECs

Our network walls are assumed to be covered by ECs, where two activities determine the net ATP flux ψ_{EC}: (i) the flow-induced ATP release by ECs, denoted below as S_{ATP}, and (ii) the ATP hydrolysis by ecto-enzymes at EC surfaces, denoted by H_{ATP}. The model

Table II. Model parameters for ATP release by RBCs

Notation	Value	Physical meaning
σ_c	0.05 Pa	Critical membrane shear stress
k_σ	700 (nM)·μm/s*	ATP release coefficient
$\dot{c}_c$	200 $\mu m^{-1}s^{-1}$	Critical curvature change rate
$k_{\dot{c}}$	0.006 μm·s	Phenomenological coefficient
$p_{\dot{c}_{max}}$	2.5	Upper limit for CFTR activation

* nM stands for nanomolar, nmol/L.

proposed by John and Barakat [62] is adopted in the present work, and the associated ATP flux is given by

$$\psi_{EC} = S_{ATP}(\sigma_w) - H_{ATP}(a_w), \tag{6}$$

where σ_w and a_w are the shear stress and the ATP concentration on the vessel walls covered by ECs, respectively. The shear-induced ATP release by ECs follows a sigmoidal dependence on shear stress, as

$$S_{ATP}(\sigma_w) = S_{max}\left[1 - exp\left(\frac{-\sigma_w}{\sigma_0}\right)\right]^3, \tag{7}$$

where S_{max} is the maximum ATP release flux, and σ_0 is a reference shear stress that regulates the rate at which the maximum ATP release flux is reached [62]. The model parameters S_{max} and σ_0 are estimated based on experimental measurements [33, 63] (see the supplementary materials for details), and their values are listed in Table III. The ATP hydrolysis rate is proportional to ATP concentration on ECs as

$$H_{ATP}(a_w) = \frac{V_{max} a_w}{K_m}, \tag{8}$$

where V_{max} is the maximum enzyme reaction rate for ATP hydrolysis, and K_m is the Michaelis constant for enzyme. The parameter values are derived from [64], as shown in Table III. As a comparison, we also consider vessel walls without ECs, where the net ATP flux is set to be 0. Thus the ATP flux on walls reads

$$D_{ATP}\frac{\partial a}{\partial \boldsymbol{n}} = \begin{cases} -\psi_{EC}, & \text{with ECs} \\ 0, & \text{without ECs} \end{cases}. \tag{9}$$

The normalized ATP release and hydrolysis by ECs are defined as

$$S^*_{ATP} = \frac{S_{ATP}\Delta L}{k_\sigma P}, H^*_{ATP} = \frac{H_{ATP}\Delta L}{k_\sigma P}, \tag{10}$$

so that they can be compared with the ATP release level of RBCs. Here ΔL is the length of a vessel wall segment.

Table III. Model parameters for ATP flux at ECs

Notation	Value	Physical meaning
S_{max}	1000 (nM)·μm/s	Maximum ATP release flux
σ_0	1 Pa	Reference shear stress
V_{max}	8×10^5 (nM)·μm/s	Maximum enzyme reaction rate for ATP hydrolysis
K_m	475000 nM	Michaelis constant for enzyme

III. RESULTS AND DISCUSSION

As discussed in Section II, the variation of ATP concentration in the network is due to the competition of two effects: (i) ATP release by RBCs and ECs and (ii) ATP hydrolysis at EC surfaces. At steady state, the ATP release is balanced by the ATP degradation as

$$\bar{\psi}^* k_\sigma P N_{RBC} + \bar{S}_{ATP} L_w = \frac{V_{max} \bar{a}_w}{K_m} L_w \approx \frac{V_{max} \bar{a}_b}{K_m} L_w, \tag{11}$$

where $\bar{\psi}^*$ is the ATP release level averaged over all RBCs, N_{RBC} is the number of RBCs, $\bar{S}_{ATP}$ is the ATP flux averaged over all vessel walls, L_w is the length of all vessel walls, and $\bar{a}_w$ and $\bar{a}_b$ are the average ATP concentration on the walls and over the whole vessel network, respectively. It should be noted that the approximate equality is obtained by assuming that $\bar{a}_w \approx \bar{a}_b$ at steady state. We will show later that this approximation is not always valid at high hematocrit. Equation 11 indicates the existence of steady state ATP concentration in blood vessel in the presence of ECs, and it is confirmed by numerical simulations, as shown in Figure 2*A*. In the presence of ECs, the average ATP concentration reaches a plateau ($\approx$ 45 nM) after long enough time, in good agreement with the value estimated by equation 11 ($\approx$ 48 nM). Note that if ECs are not taken into account, the average ATP concentration increases indefinitely with time (see Figure 2*A*, red line), since there is no degradation of ATP.

The steady state is further confirmed at different capillary number and hematocrit, as shown in Figure 2*B*–*C*. All the results fall within the order of $\sim$ 100 nM, consistent with experiments [37]. Specifically, the steady state ATP concentration is less than 10 nM when

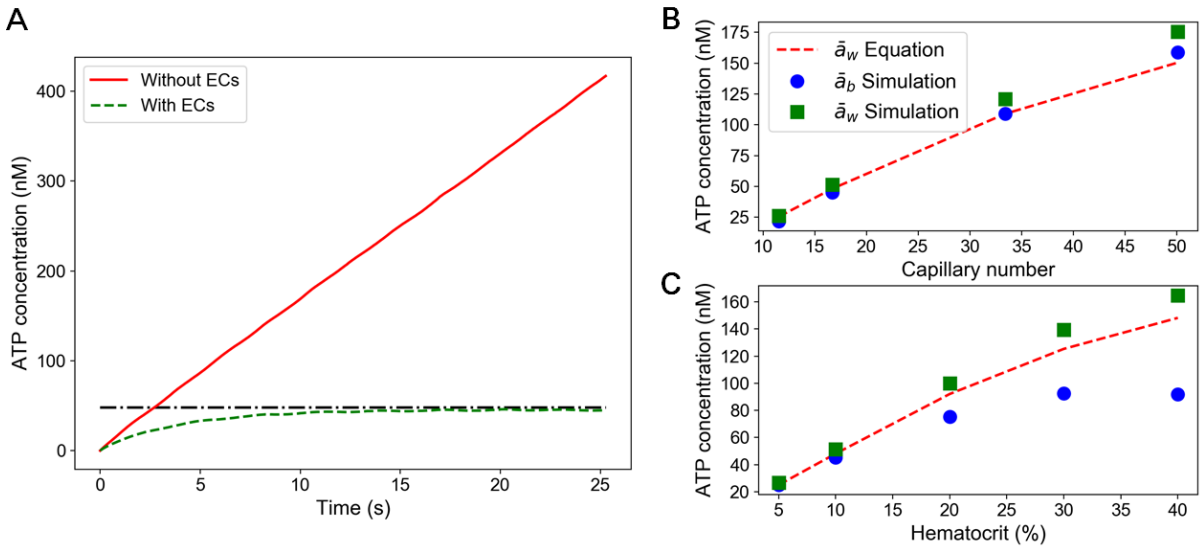

FIG. 2. *A*: Time evolution of average ATP concentration in the microvascular network at $Ht = 10\%$ and $Ca = 16.7$. The black dash-dotted line represents the value estimated by equation 11. *B*–*C*: Average ATP concentration in the microvascular network at different capillary numbers and hematocrits. The black dash-dotted line represents the value estimated by equation 11.

there is no RBCs (not shown in the figure), in good agreement with the experimental results of Yegutkin *et al.* [37]. Thus, it is reasonable to conclude that the steady state ATP concentration is a universal feature in blood vessels in the presence of ECs. This steady state prevents the indefinite increase of ATP concentration, which might be harmful to cells and tissues. Note that equation 11 constitutes a reasonable condition for steady state solution, albeit some deviations are revealed at higher hematocrit (Figure 2*B*–*C*). These deviations are attributed to the fact that the approximation $\bar{a}_w \approx \bar{a}_b$ no longer holds. A detailed explanation will be given later.

In the following subsections, we shall show that at this steady state the ATP distribution has special patterns in the microvascular network. The potential impact of ATP patterns on Ca^{2+} signaling is also discussed. Here we focus on time-averaged (or steady state) behaviors, which are obtained as follow. Initially, RBCs are randomly distributed in the network. Simulations are conducted until a steady state is established, at which the average ATP concentration in the network varies over a small range with time (as shown in Figure 2*A*). Detailed description of steady state is given in the supplementary materials. Then the simulation data during a time window T (more than 2.0 s physical time) are stored for

analysis. Unless otherwise stated, the data are averaged over time, and the term "time-averaged" is omitted hereinafter.

A. Steady state behaviors for parameters corresponding to physiological conditions

We prioritize selecting parameters that fall within the physiological range. The hematocrit is first fixed at $Ht = 10\%$, which is within the measured range of hematocrit in microcirculation[65]. The capillary number is set as $Ca = 16.7$ so that the mean velocity in the smallest vessel is about 0.2 mm/s, matching the value observed in vivo [53].

1. Impact of heteregenous hematocrit on ATP release

In a previous study, we have shown that ATP release is boosted around a simple Y-shape bifurcation [24]. To dig further into geometric effect on ATP release, we wish to highlight the fact that RBCs visiting time depends on the location in the network. For example, RBCs tend to linger more in bifurcations preceding smaller vessel diameters (due in particular to a sort of crowding effect in front of small diameter vessels). Thus, in these locations we expect a priori higher ATP release. To extract this information, the fluid domain is divided into several boxes along the flow direction (see the shaded areas in Figure 1). During a long enough time window $T \approx 2.0$ s (compared to the timescale of RBC deformation as shown in the supplementary materials), several cells (N_{local}) would have passed through a given box. We measure the ATP release level ψ_i^* and visiting time Δt_i of the ith cell in that given box, and the total ATP release by this cell is proportional to $\psi_i^* \Delta t_i$. For each box, the average level of ATP release during time period T is thus defined as

$$\psi_{local} = \frac{1}{T} \sum^{N_{local}} \psi_i^* \Delta t_i. \tag{12}$$

We refer to this quantity as local ATP release level, since it informs us on heterogeneities in the network.

The results are shown in Figure 3*A* (see also Figure S1–2 in the supplementary materials, in which similar trends are preserved at different hematocrits and flow strengths). A remarkable feature is observed: ATP release is boosted around diverging bifurcations (i.e.

B1–7, see Figure 1), similar to the results of single cell [24]. As shown in Figure 3*C*, the shear stress is high in the vicinity of the boundaries, while low in the central region. Here, the normalized shear stress σ^* is defined as the non-negative eigenvalue of the viscous stress tensor $\boldsymbol{\sigma}$ (see the supplementary materials for details). When entering a diverging bifurcation, RBCs scrape initially along the vessel wall (see Figure 1), experiencing high shear stress. After passing diverging bifurcations, these cells migrate towards the vessel center, where the shear stress is low. As a result, the ATP release exhibits a peak at the bifurcation area (Figure 3*A*).

Moreover, Figure 3*A* shows that the sudden increase of local ATP release level gets more significant at diverging bifurcations preceding smaller vessels. As stated above the changes of local ATP release level are related to accumulation of RBCs in smaller vessels. In Figure 3*A* the local hematocrit along the flow direction is shown with green dashed line. It can be seen that local ATP release level synchronizes with local hematocrit. The high local hematocrit around diverging bifurcations indicates lingering of RBCs, that the cell hangs on the apex of bifurcation without immediately entering either child vessels (see Figure 3*D*). During lingering, RBCs are exposed to high shear stress and continuously release ATP. In the supplementary materials we show the residence time of RBCs in the network (Figure S3), which is correlated with local hematocrit.

2. Role of ECs in ATP kinetics

The effects of ECs on ATP pattern are shown in Figure 3*B* (see also Figure S4–7 in the supplementary materials, in which similar trends are preserved at different hematocrits and flow strengths). For the sake of comparison with the local ATP release level of RBCs, we define the ATP release and hydrolysis by ECs within each box as

$$S_{local} = \frac{1}{T}\int_0^T S^*_{ATP}(t)dt, H_{local} = \frac{1}{T}\int_0^T H^*_{ATP}(t)dt. \tag{13}$$

Here S^*_{ATP} and H^*_{ATP} are normalized values according to equation 10 (they show the ratios of ATP release and hydrolysis by ECs over that due to RBCs), calculated over all vessel wall segments within a given box. Generally, ATP release by ECs tends towards the value corresponding to the case when there is no RBCs. Several peaks are prominent around bifurcations, both diverging and converging ones, where the shear stress is found to be higher.

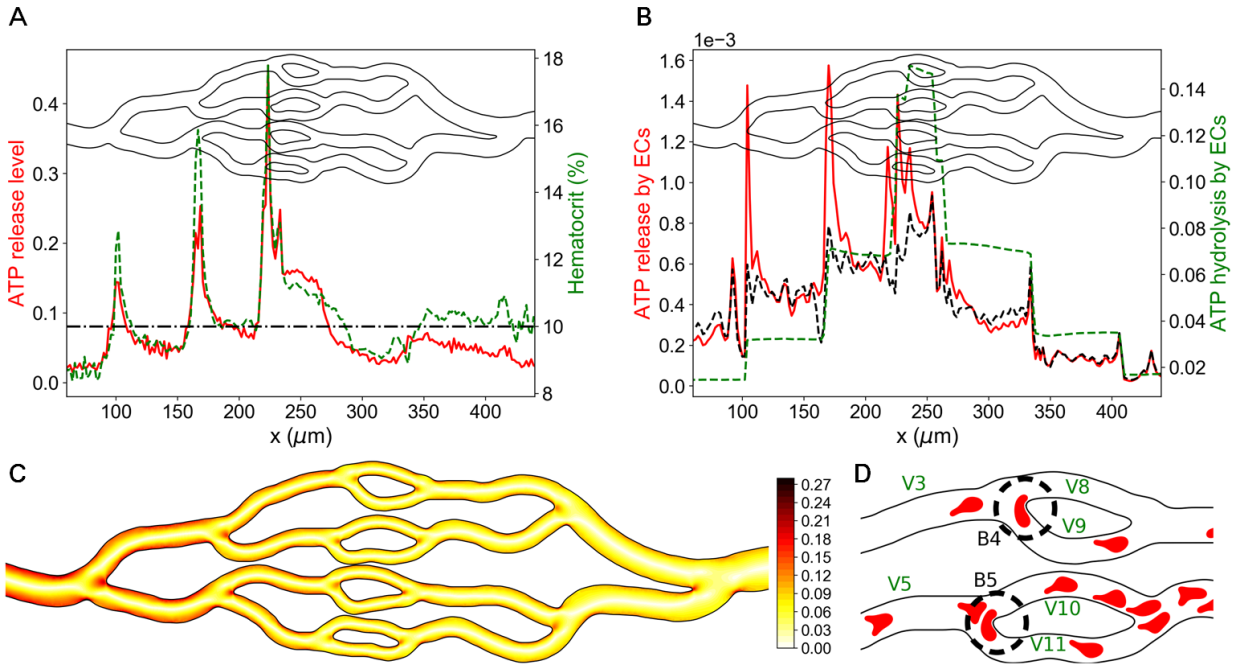

FIG. 3. Steady state ATP release and hydrolysis at $Ht = 10\%$ and $Ca = 16.7$. *A*: Local ATP release level ψ_{local} and hematocrit along the flow direction. The black dash-dotted line represents the bulk hematocrit ($Ht = 10\%$). The vessel network is plotted in black solid lines for clarity. *B*: Normalized ATP release and hydrolysis by ECs along the flow direction. The black dash line is the normalized ATP release by ECs in the absence of RBCs. These values are calculated over the vessel walls within the boxes as shown in Figure 1. *C*: Normalized shear stress σ^* (Pa) of the undisturbed flow (i.e. without RBCs). *D*: Snapshot of RBCs lingering.

This result is consistent with equation 7, according to which the ATP release rate is positively related to the shear stress. Nevertheless, the presence of RBCs can still contribute to trigger more ATP release by ECs. Indeed, the presence of RBCs affects rheological properties of blood and hence the effective shear stress felt by ECs. When RBCs are located in the core region ($x \approx 70$ and 320 μm, see Figure 3*B*), the effective viscosity of RBC suspension increases [66], thereby reducing shear stress due to RBCs suspension at vessel boundaries, hence a decline of ATP release by ECs. However, as RBCs approaches the boundaries, the viscous dissipation around these boundaries increases as well (albeit the effective average viscosity still increases due to RBCs), resulting in higher ATP release by ECs, and especially around diverging bifurcations where RBCs are very close to vessel walls ($x \approx 110$, 170 and 230 μm, see Figure 3*B*). Despite this enhanced role of RBCs in ATP release by ECs, the

relative effect of ATP release by ECs remains small, about two orders of magnitude smaller than that released by RBCs (see Figure 3*B*, where the relative value is in the 10^{-3} range). This leads us to the conclusion that the main contribution to the ATP release in vascular networks originates directly from RBCs. As for ATP hydrolysis, it sharply increases as one moves (along flow direction) towards the diverging side while it decreases on the converging side (Figure 3*B*, green dashed line). This is in phase with ATP release by RBCs, which shows the same trend (Figure 3*A*).

3. ATP pattern inside the vascular network

Hitherto, we focused on ATP release level and not on how ATP is distributed in the network due to diffusion and advection by the flow. The objective of this section is to show the spatial distribution of ATP. The simulation is run until the average ATP concentration in the network reaches steady state. This steady state results from a balance of ATP release by RBCs (and moderately by ECs) and its hyrolysis by ECs. To obtain the ATP pattern, at each sampling time the actual ATP distribution in the network is measured. This is repeated for a long time period T, and an average over time is performed. Figure 4*A* illustrates a stable pattern in the distribution of ATP throughout the network. The ATP concentration on boundaries and its distribution along flow direction are shown in Figure S8–9 of the supplementary materials. From Figure 4*A* we can summarize three trends:

(i) ATP concentration is higher in the cell free layer (CFL) close to boundaries than in the core region;

(ii) in the vicinity of diverging bifurcations, the ATP concentration is higher at the inner boundary than at the outer boundary (see the two insets of Figure 4*A*);

(iii) ATP distribution is heterogeneous among different vessels of the same level.

Trend (i) is consistent with the observation in straight channels [55], that RBCs concentrate in the core region and ATP concentrates in the periphery (CFL). In fact, besides CFL close to walls, another CFL close to centerline forms after converging bifurcations (in V20–21), as shown in Figure 4*B*. This centered CFL results from the repulsion among the cells from two upstream vessels via hydrodynamic interaction, as they meet at a converging bifurcation.

For trend (ii), we have already shown that RBCs first flow along the wall of diverging

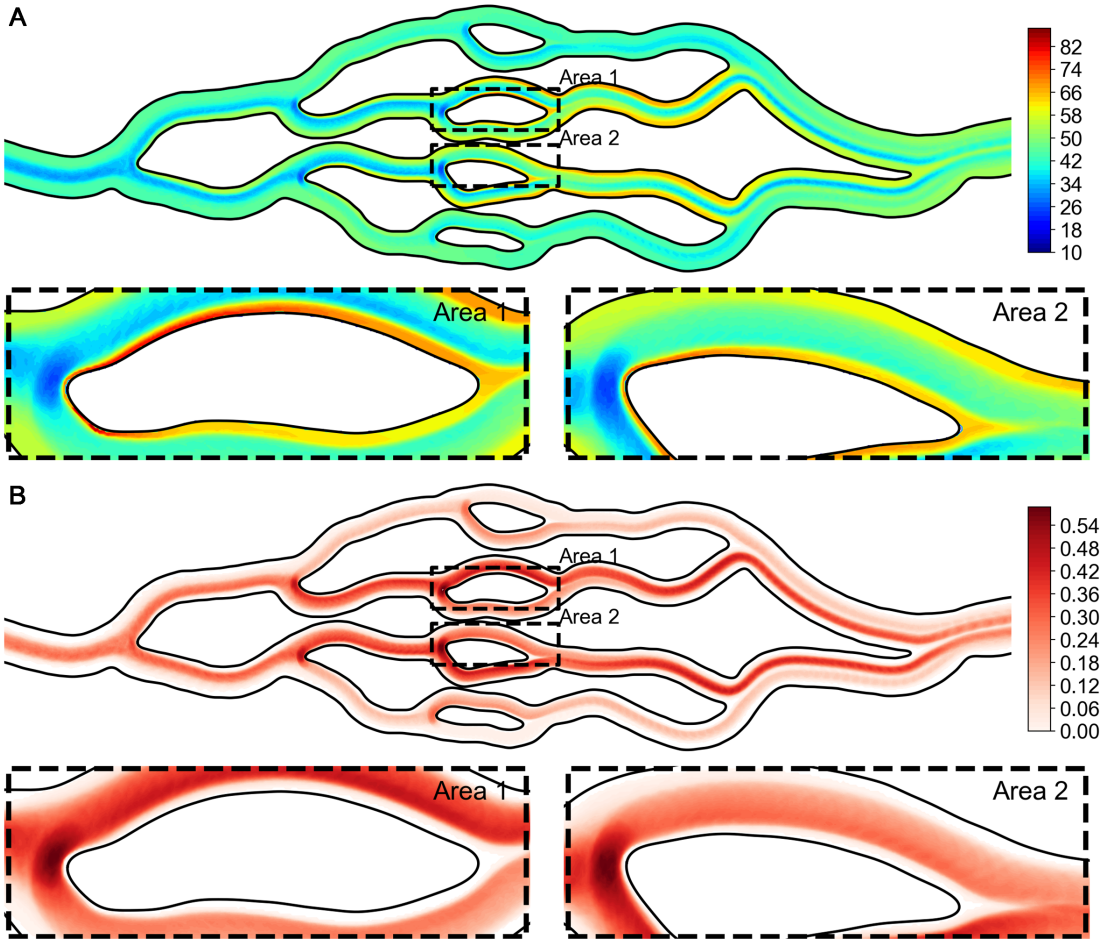

FIG. 4. A: Steady state ATP concentration (nM) and B: Steady state local hematocrit at $Ht = 10\%$ and $Ca = 16.7$. The insets show the cites where the ATP concentration is higher. The local hematocrit inside (outside) RBCs is set as 1 (0).

bifurcations, and then gradually migrate towards the central region (see Figure 1). Moreover, Figures 3A and 4B show that RBCs accumulate locally in front of diverging bifurcations, indicating the lingering effect. As a result, these cells spend more time in the high shear stress region, amplifying thus ATP release. The highest ATP concentration ($\approx$ 95 nM) is reached around the diverging bifurcations B5–6, as denoted by the insets in Figure 4A. This level of ATP concentration would induce a quite low cytoplasmic Ca^{2+} peak for ECs [67, 68], and vasodilation is not expected; but it is expected for higher hematocrits and higher flow rates, as discussed in section III B. A remark is in order. The location of high ATP concentration around diverging bifurcations is found to be slightly downstream the bifurcation apex (see Figure S8 of the supplementary material). Indeed, while the release is

maximal at bifurcations, the ATP diffuses and is advected by the flow so that the position of the maximum drifts slightly downstream.

Trend (iii) is due to biased RBC partitioning at successive bifurcations. When RBCs pass the first diverging bifurcation (B1), they flow along the inner wall, leading to a biased distribution along the cross section. When these cells reach the second diverging bifurcation (B2/3), they have not recovered to a steady distribution. The RBCs are still slowly lifting-off the wall, remaining close to the spanned wall after the impact at the bifurcation. This implies that more cells enter one child vessel (V5/6) than the other (V4/7), as shown in Figure 1. Such partitioning happens at successive bifurcations as well, and finally results in a stable but heterogeneous local hematocrit distribution as shown in Figure 4*B*. As a consequence, the ATP pattern at steady state becomes heterogeneous as well.

B. Effects of hematocrit and flow strength

In microcirculation, both flow strength as well as hematocrit can vary in vivo. For example, local hematocrit in the microvasculature can vary from 5–37% [65, 69, 70]. In polycythemia vera disease the hematocrit in macrovesssel can reach values up to 80% [71], so that its value in microcirculation is expected to be larger than the above-mentioned normal range. The flow strength depends on many factors. For example, in heart failure conditions [72], or during sport activities the flow speeds can vary significantly. This naturally raises the question of how the steady state behaviors of ATP are affected by these factors in the considered network. In this subsection, our goal is to explore this question by varying the hematocrit and the capillary number. Several regions of interest (ROI) are selected (see Figure 5*A*). In each ROI, the normalized ATP concentration by its average value in that ROI is analyzed.

1. Reduced ATP transport at high hematocrit

First, we fixed the capillary number as $Ca = 16.7$ and varied the hematocrit in a range of $Ht = 5\%$–50%. The ATP concentrations form stable patterns for different hematocrits, similar to Figure 4*A*. The three discussed trends (i)-(iii) (i.e. higher ATP concentration in CFL; ATP concentration peaks around network bifurcations; heterogeneous ATP distribu-

tion among vessels of the same level) in the previous subsection are still valid. However, the distribution of ATP is affected due to reduced ATP transport at high hematocrit, as explained below.

The main influence of hematocrit on ATP around CFL and bifurcations (trends (i) and (ii)) is the increase of heterogeneity as shown in Figure 5*D*, which results from two different causes. As shown in Ref. [55] for a straight channel, most of ATP concentration comes from RBCs close to the channel boundaries, and higher hematocrit leads to higher ATP concentration. Meanwhile, these RBCs are like barriers and slow down cross-stream ATP diffusion towards the core region. Here, we confirm this tendency in our complex network, and since we take into account consumption by ECs (unlike in [55]), we are able here to obtain the steady pattern, as shown in Figure 5*D*. It is evident that the ATP concentration is higher in CFL for all hematocrits, and its amplitude increases as the hematocrit rises. This is due to the fact that by increasing hematocrit, more and more cells are pushed towards vessel walls (Figure 5*F*), where shear stress is higher, leading to a higher ATP release. At the same time, increasing hematocrit leads to a more crowded core region by RBCs (Figure 5*F*), which constitutes barriers against ATP transport from high concentration regions (i.e. CFL) towards the center. This results thus in a more pronounced heterogeneity distribution of ATP across the vessels. This also leads to the large discrepancy between the full simulation and the analytical estimate for a high enough hematocrit, as reported in Figure 2*C*.

For ATP distribution at network boundaries, we observe an increase of ATP concentration at more upstream locations as the hematocrit increases, as shown in Figure 5*E* and *G*; the maximal value shifts to the left as hematocrit increases. This effect can be understood as follows. First, after released by RBCs, ATP is transported in two directions: stream direction and cross-stream direction (see the two arrows in Figure 5*B*). ATP is transported faster in stream direction due to advection of flow, while in cross-stream direction, the ATP transport is dominated by diffusion. As hematocrit increases, more and more cells get closer to the vessel boundaries (see Figure 5*C* and *F*), so that diffusion time becomes shorter in the cross-stream direction. In addition, at high hematocrit the flow rate decreases, reducing thus ATP advection in the stream direction. These two effects (short diffusion towards boundaries and reduction of flow rate) lead to the drift of maximal ATP towards the upstream direction.

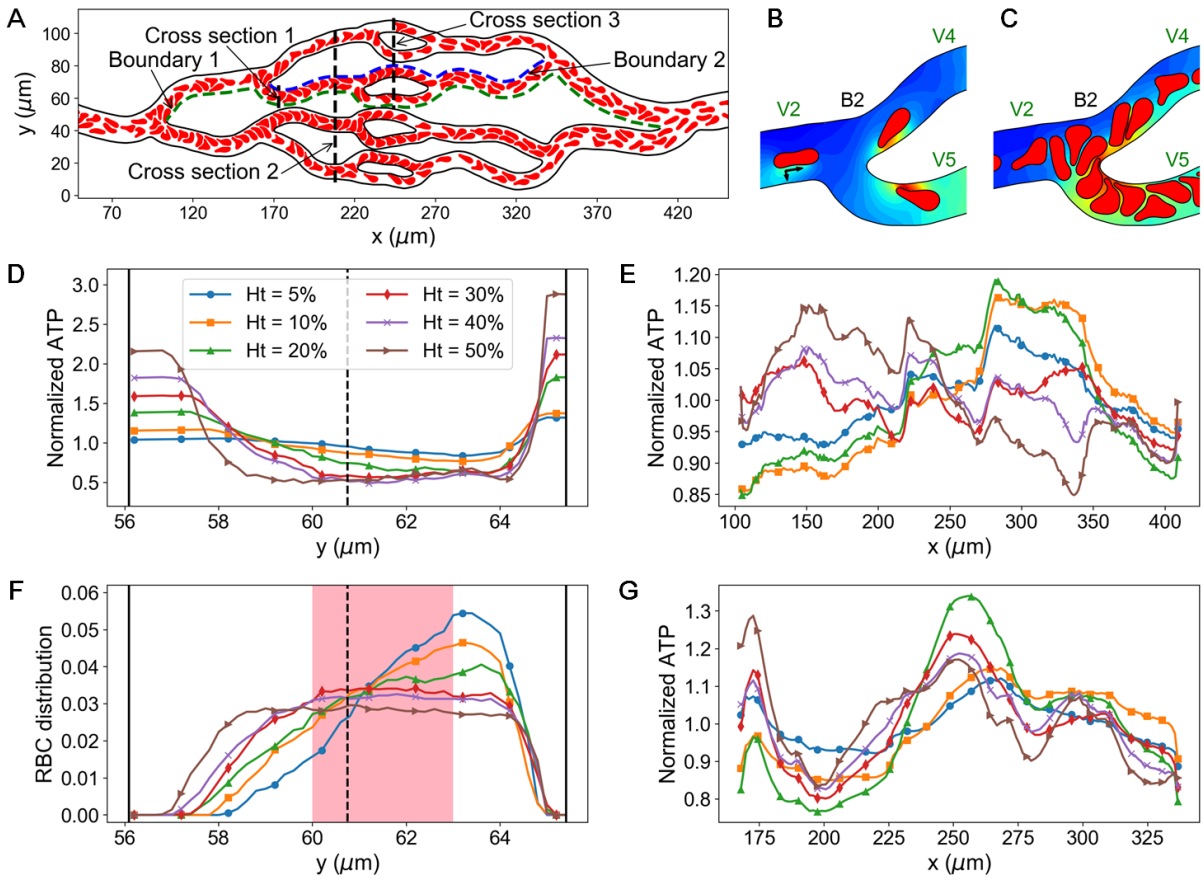

FIG. 5. *A*: Schematic of regions of interest selected for analysis. Snapshots of RBCs are plotted at $Ht = 40\%$. *B* and *C*: Instantaneous ATP concentration at $Ht = 10\%$ (*B*) and 40% (*C*). The contours represent relative ATP concentrations, with red (blue) colors denoting high (low) concentrations. The long (short) arrows represent ATP transport in stream (cross-stream) directions. *D* and *F*: Normalized ATP concentration (*D*) and RBC distribution (*F*) at cross section 1. The black solid (dashed) lines denote vessel boundaries (vessel center lines) The area labeled with pink color in *F* indicates the core region where the normalized shear stress $\sigma^* < 0.05$, lower than the critical shear stress that triggers ATP release by RBCs. The definition of RBC distribution is given in the supplementary materials. *E* and *G*: Normalized ATP concentration at boundaries 1 (*E*) and 2 (*G*).

2. *Enhanced ATP transport at high flow strength*

The effects of flow strength are studied by fixing the hematocrit at $Ht = 10\%$ and varying the capillary number in a range of $Ca = 11.5$–50.1, so that the mean velocity in

the smallest vessel is about 0.13–0.6 mm/s. High flow strength contributes to the reduction of heterogeneity among different vessels of the same level (trend (iii)), as shown in Figure 6*A* and *B*. Take bifurcation B2 as an example (see Figure 1, which is shown also in Figure 6*C*–*F*). At low flow strength, only the Px1 channels on the right side of the cell (in the frame moving with cell) in the parent vessel V2 are activated (see cell I and II in Figure 6*C* and *D*), respcetively. The ATP released by those cells (from activated parts, shown in yellow in Figure 6*C* and *D*) will predominately be advected towards the lower child vessel V5. However, as the flow strength increases a large part of the cell membrane in the parent vessel is activated for ATP release (see cell III and IV in Figure 6*E* and *F*). Therefore, it is expected that a non negligible proportion of ATP will be advected towards the upper child vessel V4, albeit the lower vessel V5 will get more ATP. Similar ATP partitioning occurs at other diverging bifurcations as well. However, no significant change of RBCs partitioning is observed.

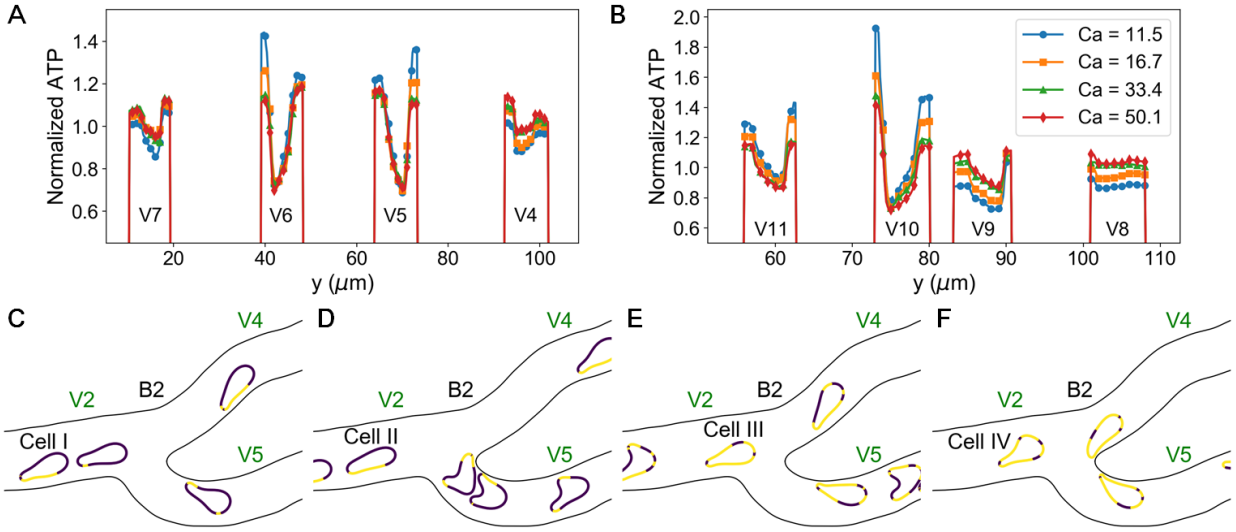

FIG. 6. *A* and *B*: Normalized ATP concentration at cross sections 2 (*A*) and 3 (*B*) (see Figure 5A for locations of cross section 2 and 3). *C*–*F*: Activation states of Px1 channels at $Ca = 11.5$ (*C*), $Ca = 16.7$ (*D*), $Ca = 33.4$ (*E*), and $Ca = 50.1$ (*F*). Light (dark) color denotes activated (inactivated) membrane location.

3. Impact on Ca^{2+} signaling

During vasomotion, the change of flow strength is accompanied with the change of hematocrit. For example, in vivo experiments have shown that the hematocrit and blood flow under muscle contraction could be more than twice than that found at rest [65]. As we have seen, higher hematocrit and flow strength are two factors that favor ATP release from RBCs. The released ATP can react with ECs receptors (e.g. purigenic receptors), a first stage that elicit cascade of reactions leading to Ca^{2+} and NO (a vasodilator) signaling from ECs. Experimental studies reported that Ca^{2+} responses in ECs were observed when extracellular ATP concentration was higher than 250 nM [67]. Here, we take this value as the threshold ATP concentration for Ca^{2+} signaling activation. The question addressed below is to determine both the flow strength and hematocrit that are needed in order to obtain this ATP threshold.

With the increase of hematocrit and flow strength, the ATP concentration on vessel boundaries increases (see Figure 2*B* and *C*), and eventually reaches the threshold at some critical hematocrit. Due to the heterogeneity of ATP distribution, the critical hematocrit varies on network boundaries, as shown in Figure 7*A*. Apparently, ECs get activated at lower hematocrit if there are more cells, for example near diverging bifurcations and centered vessels (the green lines in Figure 7*A*). By increasing the flow strength, the critical hematocrit is greatly reduced, as shown by the dashed lines in Figure 7*A*.

Moreover, we notice that only the boundaries of the smallest vessel V10 are activated at moderate hematocrit and flow strength ($Ht = 20\%$, $Ca = 16.7$). Note that our vascular network corresponds rather to a capillary network, where blood vessels are devoid of smooth muscle cells, meaning that no vasodilation can take place there. Since vessel V10 is far from the inlet of the network, Ca^{2+} signal would propagate a long distance, and becomes weak before reaching upstream arterioles [73]. As hematocrit increases, more ATP accumulates at upstream bifurcations. Ca^{2+} is expected to be triggered close to the inlet of the network (purple and brown lines in Figure 7*B*), that is close to the end of arteriole trees. Propagation of Ca^{2+} signal upstream would require traveling over a short distance before reaching arterioles. Given the reported speeds of Ca^{2+} propagation (at least 10 μm/s [73]), few seconds are needed for Ca^{2+} to reach the end of arteriole tree.

Let us quantify the proportion of network boundaries which are potentially activated with regard to Ca^{2+} signaling. As stated above, we expect this signaling to take place when ATP concentration exceeds 250 nM. The proportion of activated boundaries is defined

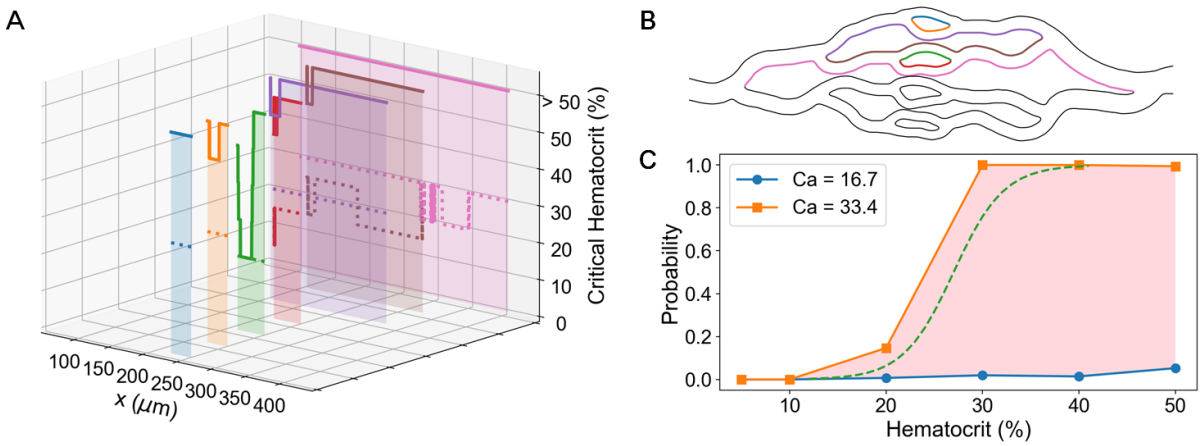

FIG. 7. *A*: Critical hematocrit on network boundaries at which the Ca^{2+} signaling in ECs would be activated ($a_w \geq 250$ nM). The capillary numbers are $Ca = 16.7$ (solid lines) and $Ca = 33.4$ (dashed lines). The colors indicate the boundaries of interest as shown in *B*. Only the top half boundaries are shown for clarity. *C*: Probability of Ca^{2+} signaling on network boundaries as a function of hematocrit. The dashed line indicates the probability of Ca^{2+} signaling due to stimulation (e.g. muscle contraction), as the hematocrit and flow strength increase simultaneously (drawn by hand).

as the ratio of activated boundaries over the total length including all boundaries within the network (excluding inlet and outlet vessels). This proportion is referred to as the the probability of Ca^{2+} signaling. As shown in Figure 7*C*, the probability of Ca^{2+} signaling behaves like a sigmoid function. It is quite intuitive that higher capillary number and higher hematocrit result in more activated ECs (larger probability). In capillary networks $Ca = 16.7$ and 33.4 correspond to shear stress at the walls of about 0.3 and 0.6 Pa, which reaches the lower limit of typical physiological values (approximately 0.5–5 Pa) [74, 75]. In resting circumstance, hematocrit in microcirculations is usually in the range 5-20% [65, 69]. According to Figure 7*C*, this may mean that the propability of Ca^{2+} signaling is small. However, under stimulation like muscle contraction, both hematocrit and flow strength increase (hematocrit can be two fold larger [65]), increasing thus significantly the probability of Ca^{2+} activation.

IV. CONCLUSION

In this work, we extend the previous studies of ATP release by RBCs in straight channels [24, 55] to a microvascular network. This work also contributes by considering the role of ECs in ATP kinetics. Non-trivial ATP release by RBCs and heterogeneous ATP patterns are observed due to the network geometry, which are influenced by hematocrit and flow strength.

We first showed that the presence of ECs leads to a steady state ATP pattern. This stable ATP pattern is a hallmark of cell partitioning at successive diverging bifurcations. This partitioning greatly alters RBCs lateral position in vessels, as well as ATP release by RBCs. The ATP degradation by ECs is essential in order to establish a stable ATP pattern, but its release by ECs is not significant as compared to that of RBCs. High ATP concentration is observed in CFL and around diverging bifurcations, which might be beneficial to Ca^{2+} signaling of ECs [8, 10]. Whether or not a high level of ATP at bifurcations (and thus an initiation Ca^{2+} release there) has a documented physiological implication is, to our best knowledge, not known at present.

Upon changing hematocrit and flow strength different ATP patterns are observed. Indeed, high hematocrit reduces the ATP transport towards downstream vessels, so that the location of ATP-induced Ca^{2+} signaling is expected to be shifted towards upstream vessels. Regarding the effect of flow strength, we observe a reduction of heterogeneity of ATP distribution due to enhanced ATP transport. Certain diseases like polycythemia vera [76, 77] and anemia [78] are accompanied by a significant modification of hematocrit and of flow strength (due to a change of effective viscosity [79]). It would be an interesting task for future studies to elucidate the impact on chemical signaling (ATP, Ca^{2+} and NO) related to these diseases.

An interesting conclusion from our study is that blood flow in vascular networks is not a simple summation of the flows in a series of straight channels. Indeed, the structure of the network, like bifurcations, plays an important role in RBC dynamics as well as in chemical signaling. Here, we focused on a topologically symmetric network (successive regular splitting of parent vessel into two child vessels). How ATP signaling behaves in a more complex geometry is an interesting, albeit challenging, work for the future.

Another perspective concerns the impact of abnormal cells in biochemical signaling. Some

diseases, like sickle cell anemia, affect RBC morphology and flexibility [80, 81]. This will in turn influence cell response to fluid stress, which may thus alter ATP release level. Moreover, a dysfunction of transmembrane channels and enzymes can have an influence on ATP signaling as well. For example, mefloquine, known as an anti-malarial medicine, can block the Px1 channel [82]. It is also known that some drugs act as inhibitors of ecto-enzymes [83] (which may lead to a reduction of ATP hydrolysis). A systematic analysis of ATP kinetics by abnormal cells should be performed in order to determine the main consequences.

ACKNOWLEDGEMENTS

We thank CNES (Centre National d'Etudes Spatiales) for financial support and for having access to data of microgravity, and the French-German university programme "Living Fluids" (Grant CFDA-Q1-14) for financial support. All the computations presented in this paper were performed using the GRICAD infrastructure (https://gricad.univ-grenoble-alpes.fr), which is supported by Grenoble research communities.

---

[1] T. Forrester and A. R. Lind, "Identification of adenosine triphosphate in human plasma and the concentration in the venous effluent of forearm muscles before, during and after sustained contractions," J Physiol **204**, 347–64 (1969).

[2] G. R. Bergfeld and T. Forrester, "Release of atp from human erythrocytes in response to a brief period of hypoxia and hypercapnia," Cardiovasc Res **26**, 40–7 (1992).

[3] P. Bodin and G. Burnstock, "Synergistic effect of acute hypoxia on flow-induced release of atp from cultured endothelial cells," Experientia **51**, 256–9 (1995).

[4] S. P. Mortensen, J. Gonzalez-Alonso, L. T. Bune, B. Saltin, H. Pilegaard, and Y. Hellsten, "Atp-induced vasodilation and purinergic receptors in the human leg: roles of nitric oxide, prostaglandins, and adenosine," Am J Physiol Regul Integr Comp Physiol **296**, R1140–8 (2009).

[5] M. Billaud, A. W. Lohman, A. C. Straub, R. Looft-Wilson, S. R. Johnstone, C. A. Araj, A. K. Best, F. B. Chekeni, K. S. Ravichandran, S. Penuela, D. W. Laird, and B. E. Isakson, "Pannexin1 regulates alpha1-adrenergic receptor-mediated vasoconstriction," Circ Res **109**,

80–5 (2011).

[6] W. K. Lim To, P. Kumar, and J. M. Marshall, "Hypoxia is an effective stimulus for vesicular release of atp from human umbilical vein endothelial cells," Placenta **36**, 759–66 (2015).

[7] K. Yamamoto, R. Korenaga, A. Kamiya, Z. Qi, M. Sokabe, and J. Ando, "P2x(4) receptors mediate atp-induced calcium influx in human vascular endothelial cells," Am J Physiol Heart Circ Physiol **279**, H285–92 (2000).

[8] S. Xu, X. Li, K. B. LaPenna, S. D. Yokota, S. Huke, and P. He, "New insights into shear stress-induced endothelial signalling and barrier function: cell-free fluid versus blood flow," Cardiovasc Res **113**, 508–518 (2017).

[9] D. E. Brooks, J. W. Goodwin, and G. V. F. Seaman, "Interactions among erythrocytes under shear," Journal of Applied Physiology **28** (1970).

[10] M. J. Plank, D. J. Wall, and T. David, "Atherosclerosis and calcium signalling in endothelial cells," Prog Biophys Mol Biol **91**, 287–313 (2006).

[11] A. R. Crecelius, B. S. Kirby, J. C. Richards, L. J. Garcia, W. F. Voyles, D. G. Larson, G. J. Luckasen, and F. A. Dinenno, "Mechanisms of atp-mediated vasodilation in humans: modest role for nitric oxide and vasodilating prostaglandins," Am J Physiol Heart Circ Physiol **301**, H1302–10 (2011).

[12] M. D. Sweeney, S. Ayyadurai, and B. V. Zlokovic, "Pericytes of the neurovascular unit: key functions and signaling pathways," Nat Neurosci **19**, 771–83 (2016).

[13] J. Almaca, J. Weitz, R. Rodriguez-Diaz, E. Pereira, and A. Caicedo, "The pericyte of the pancreatic islet regulates capillary diameter and local blood flow," Cell Metab **27**, 630–644 e4 (2018).

[14] R. S. Sprague, M. L. Ellsworth, A. H. Stephenson, and A. J. Lonigro, "Atp: the red blood cell link to no and local control of the pulmonary circulation," Am J Physiol **271**, H2717–2722 (1996).

[15] R. S. Sprague, M. L. Ellsworth, A. H. Stephenson, M. E. Kleinhenz, and A. J. Lonigro, "Deformation-induced atp release from red blood cells requires cftr activity," Am J Physiol **275**, H1726–32 (1998).

[16] D. J. Fischer, N. J. Torrence, R. J. Sprung, and D. M. Spence, "Determination of erythrocyte deformability and its correlation to cellular atp release using microbore tubing with diameters that approximate resistance vessels in vivo," Analyst **128**, 1163–8 (2003).

[17] J. Wan, W. D. Ristenpart, and H. A. Stone, "Dynamics of shear-induced atp release from red blood cells," Proc Natl Acad Sci U S A **105**, 16432–7 (2008).

[18] Alison M. Forsyth, Jiandi Wan, Philip D. Owrutsky, Manouk Abkarian, and Howard A. Stone, "Multiscale approach to link red blood cell dynamics, shear viscosity, and atp release," Proc. Natl. Acad. Sci. USA. **108**, 10986–10991 (2011).

[19] C. D'Hondt, R. Ponsaerts, H. De Smedt, M. Vinken, E. De Vuyst, M. De Bock, N. Wang, V. Rogiers, L. Leybaert, B. Himpens, and G. Bultynck, "Pannexin channels in atp release and beyond: an unexpected rendezvous at the endoplasmic reticulum," Cell Signal **23**, 305–16 (2011).

[20] L. Bao, S. Locovei, and G. Dahl, "Pannexin membrane channels are mechanosensitive conduits for atp," FEBS Lett **572**, 65–8 (2004).

[21] S. Locovei, L. Bao, and G. Dahl, "Pannexin 1 in erythrocytes: Function without a gap," Proc Natl Acad Sci U S A **103**, 7655–7659 (2006).

[22] G. M. Braunstein, R. M. Roman, J. P. Clancy, B. A. Kudlow, A. L. Taylor, V. G. Shylonsky, B. Jovov, K. Peter, T. Jilling, II Ismailov, D. J. Benos, L. M. Schwiebert, J. G. Fitz, and E. M. Schwiebert, "Cystic fibrosis transmembrane conductance regulator facilitates atp release by stimulating a separate atp release channel for autocrine control of cell volume regulation," J Biol Chem **276**, 6621–30 (2001).

[23] B. Chasan, N. A. Geisse, K. Pedatella, D. G. Wooster, M. Teintze, M. D. Carattino, W. H. Goldmann, and H. F. Cantiello, "Evidence for direct interaction between actin and the cystic fibrosis transmembrane conductance regulator," Eur Biophys J **30**, 617–24 (2002).

[24] H. Zhang, Z. Shen, B. Hogan, A. I. Barakat, and C. Misbah, "Atp release by red blood cells under flow: Model and simulations," Biophys J **115**, 2218–2229 (2018).

[25] S. P. Olesen, D. E. Clapham, and P. F. Davies, "Haemodynamic shear stress activates a k+ current in vascular endothelial cells," Nature **331**, 168–70 (1988).

[26] A. I. Barakat, E. V. Leaver, P. A. Pappone, and P. F. Davies, "A flow-activated chloride-selective membrane current in vascular endothelial cells," Circ Res **85**, 820–8 (1999).

[27] Jr. Dewey, C. F., S. R. Bussolari, Jr. Gimbrone, M. A., and P. F. Davies, "The dynamic response of vascular endothelial cells to fluid shear stress," J Biomech Eng **103**, 177–85 (1981).

[28] G. Helmlinger, R. V. Geiger, S. Schreck, and R. M. Nerem, "Effects of pulsatile flow on cultured vascular endothelial cell morphology," J Biomech Eng **113**, 123–31 (1991).

[29] M. Inglebert, L. Locatelli, D. Tsvirkun, P. Sinha, J. A. Maier, C. Misbah, and L. Bureau, "The effect of shear stress reduction on endothelial cells: A microfluidic study of the actin cytoskeleton," Biomicrofluidics **14**, 024115 (2020).

[30] R. O. Dull and P. F. Davies, "Flow modulation of agonist (atp)-response (ca2+) coupling in vascular endothelial cells," Am J Physiol **261**, H149–54 (1991).

[31] J. Shen, F. W. Luscinskas, A. Connolly, Jr. Dewey, C. F., and Jr. Gimbrone, M. A., "Fluid shear stress modulates cytosolic free calcium in vascular endothelial cells," Am J Physiol **262**, C384–90 (1992).

[32] P. Milner, K. A. Kirkpatrick, V. Ralevic, V. Toothill, J. Pearson, and G. Burnstock, "Endothelial cells cultured from human umbilical vein release atp, substance p and acetylcholine in response to increased flow," Proc Biol Sci **241**, 245–8 (1990).

[33] K. Yamamoto, T. Sokabe, N. Ohura, H. Nakatsuka, A. Kamiya, and J. Ando, "Endogenously released atp mediates shear stress-induced ca2+ influx into pulmonary artery endothelial cells," Am J Physiol Heart Circ Physiol **285**, H793–803 (2003).

[34] K. Yamamoto, K. Furuya, M. Nakamura, E. Kobatake, M. Sokabe, and J. Ando, "Visualization of flow-induced atp release and triggering of ca2+ waves at caveolae in vascular endothelial cells," J Cell Sci **124**, 3477–83 (2011).

[35] E. R. Lazarowski, R. C. Boucher, and T. K. Harden, "Mechanisms of release of nucleotides and integration of their action as p2x- and p2y-receptor activating molecules," Mol Pharmacol **64**, 785–95 (2003).

[36] Erik M. Schwiebert and Akos Zsembery, "Extracellular atp as a signaling molecule for epithelial cells," Biochimica et Biophysica Acta (BBA) - Biomembranes **1615**, 7–32 (2003).

[37] G. Yegutkin, P. Bodin, and G. Burnstock, "Effect of shear stress on the release of soluble ecto-enzymes atpase and 5'-nucleotidase along with endogenous atp from vascular endothelial cells," Br J Pharmacol **129**, 921–6 (2000).

[38] L. M. Schwiebert, W. C. Rice, B. A. Kudlow, A. L. Taylor, and E. M. Schwiebert, "Extracellular atp signaling and p2x nucleotide receptors in monolayers of primary human vascular endothelial cells," Am J Physiol Cell Physiol **282**, C289–301 (2002).

[39] G. Burnstock and A. Verkhratsky, "Long-term (trophic) purinergic signalling: purinoceptors control cell proliferation, differentiation and death," Cell Death Dis **1**, e9 (2010).

[40] K. Svanes and B. W. Zweifach, "Variations in small blood vessel hematocrits produced in hypothermic rats by micro-occlusion," Microvasc Res **1**, 210–220 (1968).

[41] Y. C. Fung, "Stochastic flow in capillary blood vessels," Microvasc Res **5**, 34–48 (1973).

[42] X. Yin, T. Thomas, and J. Zhang, "Multiple red blood cell flows through microvascular bifurcations: cell free layer, cell trajectory, and hematocrit separation," Microvasc Res **89**, 47–56 (2013).

[43] J. M. Sherwood, D. Holmes, E. Kaliviotis, and Balabani S., "Spatial distributions of red blood cells significantly alter local haemodynamics," PLoS ONE **9** (2014), https://doi.org/10.1371/journal.pone.0100473.

[44] Zaiyi Shen, Gwennou Coupier, Badr Kaoui, BenoÃ®t Polack, Jens Harting, Chaouqi Misbah, and Thomas Podgorski, "Inversion of hematocrit partition at microfluidic bifurcations," Microvascular Research **105**, 40–46 (2016).

[45] N. Tousi, B. Wang, K. Pant, M. F. Kiani, and B. Prabhakarpandian, "Preferential adhesion of leukocytes near bifurcations is endothelium independent," Microvasc Res **80**, 384–8 (2010).

[46] B. Prabhakarpandian, Y. Wang, A. Rea-Ramsey, S. Sundaram, M. F. Kiani, and K. Pant, "Bifurcations: focal points of particle adhesion in microvascular networks," Microcirculation **18**, 380–9 (2011).

[47] G. Lamberti, F. Soroush, A. Smith, M. F. Kiani, B. Prabhakarpandian, and K. Pant, "Adhesion patterns in the microvasculature are dependent on bifurcation angle," Microvasc Res **99**, 19–25 (2015).

[48] A. M. Malek, S. L. Alper, and S. Izumo, "Hemodynamic shear stress and its role in atherosclerosis," JAMA **282**, 2035–42 (1999).

[49] A. Comerford, T. David, and M. Plank, "Effects of arterial bifurcation geometry on nucleotide concentration at the endothelium," Ann Biomed Eng **34**, 605–17 (2006).

[50] A. Comerford, M. J. Plank, and T. David, "Endothelial nitric oxide synthase and calcium production in arterial geometries: an integrated fluid mechanics/cell model," J Biomech Eng **130**, 011010 (2008).

[51] Peter Balogh and Prosenjit Bagchi, "Analysis of red blood cell partitioning at bifurcations in simulated microvascular networks," Physics of Fluids **30**, 051902 (2018).

[52] Q. Zhou, J. Fidalgo, M. O. Bernabeu, M. S. N. Oliveira, and T. Kruger, "Emergent cell-free layer asymmetry and biased haematocrit partition in a biomimetic vascular network of

successive bifurcations," Soft Matter **17**, 3619–3633 (2021).

[53] Aleksander S Popel and Paul C Johnson, "Microcirculation and hemorheology," Annu. Rev. Fluid Mech. **37**, 43–69 (2005).

[54] C. G. Ellis, S. Milkovich, and D. Goldman, "What is the efficiency of atp signaling from erythrocytes to regulate distribution of o(2) supply within the microvasculature?" Microcirculation **19**, 440–50 (2012).

[55] Z. Gou, H. Zhang, M. Abbasi, and C. Misbah, "Red blood cells under flow show maximal atp release for specific hematocrit," Biophysical Journal **120**, 4819–4831 (2021).

[56] Z. Y. Shen, A. Farutin, M. Thiebaud, and C. Misbah, "Interaction and rheology of vesicle suspensions in confined shear flow," Physical Review Fluids **2** (2017), ARTN 103101 10.1103/PhysRevFluids.2.103101.

[57] H. D. Zhang and C. Misbah, "Lattice boltzmann simulation of advection-diffusion of chemicals and applications to blood flow," Computers & Fluids **187**, 46–59 (2019).

[58] Peter Balogh and Prosenjit Bagchi, "Direct numerical simulation of cellular-scale blood flow in 3d microvascular networks," Biophysical Journal **113**, 2815–2826 (2017).

[59] Ou-Yang Zhong-Can and Wolfgang Helfrich, "Bending energy of vesicle membranes: General expressions for the first, second, and third variation of the shape energy and applications to spheres and cylinders," Phys. Rev. A **39**, 5280 (1989).

[60] Giovanni Ghigliotti, Thierry Biben, and Chaouqi Misbah, "Rheology of a dilute two-dimensional suspension of vesicles," Journal of Fluid Mechanics **653**, 489–518 (2010).

[61] B. Kaoui, G. H. Ristow, I. Cantat, C. Misbah, and W. Zimmermann, "Lateral migration of a two-dimensional vesicle in unbounded poiseuille flow," Phys Rev E Stat Nonlin Soft Matter Phys **77**, 021903 (2008).

[62] K. John and A. I. Barakat, "Modulation of atp/adp concentration at the endothelial surface by shear stress: effect of flow-induced atp release," Ann Biomed Eng **29**, 740–51 (2001).

[63] P. Bodin and G. Burnstock, "Evidence that release of adenosine triphosphate from endothelial cells during increased shear stress is vesicular," J Cardiovasc Pharmacol **38**, 900–8 (2001).

[64] N. J. Cusack, J. D. Pearson, and J. L. Gordon, "Stereoselectivity of ectonucleotidases on vascular endothelial cells," Biochem J **214**, 975–81 (1983).

[65] B. Klitzman and B. R. Duling, "Microvascular hematocrit and red cell flow in resting and contracting striated muscle," Am J Physiol **237**, H481–90 (1979).

[66] M. Thiebaud and C. Misbah, "Rheology of a vesicle suspension with finite concentration: a numerical study," Phys Rev E Stat Nonlin Soft Matter Phys **88**, 062707 (2013).

[67] K. Yamamoto, R. Korenaga, A. Kamiya, and J. Ando, "Fluid shear stress activates ca(2+) influx into human endothelial cells via p2x4 purinoceptors," Circ Res **87**, 385–91 (2000).

[68] A. K. Nayak, Z. Gou, S. L. Das, A. I. Barakat, and C. Misbah, "Mathematical modeling of intracellular calcium in presence of receptor: a homeostatic model for endothelial cell," Biomech Model Mechanobiol (2022), 10.1007/s10237-022-01643-9.

[69] I. H. Sarelius, D. N. Damon, and B. R. Duling, "Microvascular adaptations during maturation of striated muscle," Am J Physiol **241**, H317–24 (1981).

[70] I. H. Sarelius and B. R. Duling, "Direct measurement of microvessel hematocrit, red cell flux, velocity, and transit time," Am J Physiol **243**, H1018–26 (1982).

[71] Arif H. Kamal and Philip R. Greipp, "Systemic capillary leak syndrome mimicking polycythemia vera," Blood **108**, 3599–3726 (2006).

[72] Theresa A McDonagh, Marco Metra, Marianna Adamo, Roy S Gardner, Andreas Baumbach, Michael Böhm, Haran Burri, Javed Butler, Jelena Čelutkienė, Ovidiu Chioncel, John G F Cleland, Andrew J S Coats, Maria G Crespo-Leiro, Dimitrios Farmakis, Martine Gilard, Stephane Heymans, Arno W Hoes, Tiny Jaarsma, Ewa A Jankowska, Mitja Lainscak, Carolyn S P Lam, Alexander R Lyon, John J V McMurray, Alexandre Mebazaa, Richard Mindham, Claudio Muneretto, Massimo Francesco Piepoli, Susanna Price, Giuseppe M C Rosano, Frank Ruschitzka, Anne Kathrine Skibelund, and ESC Scientific Document Group, "2021 esc guidelines for the diagnosis and treatment of acute and chronic heart failure: Developed by the task force for the diagnosis and treatment of acute and chronic heart failure of the european society of cardiology (esc) with the special contribution of the heart failure association (hfa) of the esc," European Heart Journal **42**, 4909–4909 (2021).

[73] J. Long, M. Junkin, P. K. Wong, J. Hoying, and P. Deymier, "Calcium wave propagation in networks of endothelial cells: model-based theoretical and experimental study," PLoS Comput Biol **8**, e1002847 (2012).

[74] H. H. Lipowsky, S. Kovalcheck, and B. W. Zweifach, "The distribution of blood rheological parameters in the microvasculature of cat mesentery," Circ Res **43**, 738–49 (1978).

[75] I. H. Sarelius, "Cell and oxygen flow in arterioles controlling capillary perfusion," Am J Physiol **265**, H1682–7 (1993).

[76] H. K. Steinman, A. Kobza-Black, T. M. Lotti, L. Brunetti, E. Panconesi, and M. W. Greaves, "Polycythaemia rubra vera and water-induced pruritus: blood histamine levels and cutaneous fibrinolytic activity before and after water challenge," Br J Dermatol **116**, 329–33 (1987).

[77] Y. Inami, M. Fukushima, T. Kume, and D. Uta, "Histamine enhances atp-induced itching and responsiveness to atp in keratinocytes," J Pharmacol Sci **148**, 255–261 (2022).

[78] S. J. Hayden, T. J. Albert, T. R. Watkins, and E. R. Swenson, "Anemia in critical illness: insights into etiology, consequences, and management," Am J Respir Crit Care Med **185**, 1049–57 (2012).

[79] P. Cabrales, "Effects of erythrocyte flexibility on microvascular perfusion and oxygenation during acute anemia," Am J Physiol Heart Circ Physiol **293**, H1206–15 (2007).

[80] H. Lei and G. E. Karniadakis, "Probing vasoocclusion phenomena in sickle cell anemia via mesoscopic simulations," Proc Natl Acad Sci U S A **110**, 11326–30 (2013).

[81] Russell E. Ware, Mariane de Montalembert, LÃ©on Tshilolo, and Miguel R. Abboud, "Sickle cell disease," The Lancet **390**, 311–323 (2017).

[82] R. Iglesias, D. C. Spray, and E. Scemes, "Mefloquine blockade of pannexin1 currents: resolution of a conflict," Cell Commun Adhes **16**, 131–7 (2009).

[83] Y. Baqi, "Ecto-nucleotidase inhibitors: recent developments in drug discovery," Mini Rev Med Chem **15**, 21–33 (2015).